Experimental investigations of a swirling jet in stationary and rotating surroundings

By HANZHUANG LIANG AND T. MAXWORTHY

Department of Aerospace and Mechanical Engineering, University of Southern California, CA 90089, USA

(Received ??)

The 'plug' flow emerging from a long tube, which was rotating with speed $\Omega\,\mathrm{s}^{-1}$ and with an exit of radius R, into a large stationary reservoir was used in the experimental investigation of swirling jets. Moderate Reynolds numbers, $Re = 600$–2000, were studied, and swirl numbers, S, the ratio of nozzle exit rotational speed, ΩR, to the mean mass axial velocity, U, were in the range 0–1.1. Four regimes were covered: non-swirling jets, weakly swirling jets, strongly swirling jets before vortex breakdown and stable vortex breakdown. Kelvin–Helmholtz (k–H) instability in the axial shear-layer, leading to vortex ring formation with $m = 0$, dominated non-swirling and weakly swirling jets. After the introduction of sufficient rotation, co-rotating, counter-winding helical waves with $m = +2$ or $+3$ replaced vortex rings to become the dominant vortex structure. After vortex breakdown, strong helical waves with $m = +1$ and $+2$ coexisted, with $m = +1$ being dominant. The differences between the measured and calculated vortex pitch angles and the direction of the vortex lines of the mean flow suggest that the centrifugal instability of the axial vorticity distribution displace the helical waves towards the co-winding direction. The high fluctuation level in the shear-layer, the location of the fully turbulent region further upstream, the rapid spreading of the highly turbulent shear-layer and the enhanced entrainment of the reservoir fluid by the jet, make swirling jets very different from non-swirling ones, especially after vortex breakdown.

A quantitative visualization study has been carried for cases where the reservoir was rotating independently with $S_a = \Omega_a R/U = \pm 0.35$, ± 0.51 and ± 0.70 at $Re = 1000$ and 2000, where Ω_a is the rotation rate of the reservoir. Some mean flow characteristics, such as the criteria for breakdown and the axial distance between the stagnation point and the nozzle exit, were found to be mainly dependent on the absolute swirl number of the jet, S. The criterion for vortex breakdown was found to be only slightly different in stationary, co- and counter-swirl surroundings. Thus it appears that the flow criticality, i.e., transition to vortex breakdown, depends mainly on the velocity distributions of the vortex core, while instabilities resulting from the swirl difference between the jet and its ambient seem to have only a secondary effect. An attempt is made to reconcile these results with existing theory and experiments.

1. Introduction

This paper supplements the work reported in Liang & Maxworthy (2004) (hereafter LM) which focused on the details of the instability mechanisms found in swirling jets and their convective/absolute, local/global and linear/nonlinear characteristics. Such flows represent one of a basic handful of examples that, while of great practical significance, allow for the fundamental study of complex but generic dynamical processes and their

interactions. They feature prominently in a variety of propulsion and combustion systems. The efficiency of chemical reactors and mixing devices is enhanced by making use of the faster spreading and more rapid mixing of swirling jet. Atmospheric conditions can give rise to swirling flows, e.g. tornados, dust devils and water spouts, while they are necessary feature of aircraft wake flows.

The need for performance enhancement and optimization makes desirable an improved understanding of the interaction of the competing dynamical mechanisms that arise in swirling jets and govern their evolution. Their axial velocity profiles allow for shear-induced instabilities similar to those encountered in non-swirling flows. However, the additional presence of swirl can result in an azimuthal shear-layer and centrifugal instability when the circulation decreases outwards. When the swirl rate is high enough, swirling jets are known to produce vortex breakdown events, which are characterized by abrupt flow changes, a stagnation point followed by a region of reverse flow and highly turbulent flow. One of several attempts to describe the basic physics of this important generic phenomenon is given in Gupta, Lilley & Syred (1984) and are also reviewed in Hall (1972), Leibovich (1978), Leibovich (1983) and Escudier (1987). However a universally accepted explanation of its fundamental nature still remains elusive. Up to now it was thought that two forms of vortex breakdown exist: the *near-axisymmetric* and the *spiral* type, first described by Lambourne & Bryer (1961), although a number of other types have been observed, e.g. by Sarpkaya (1971). However, such a seemingly fundamental categorisation is by no means certain and open to further interpretation.

Before the late 1980's, the major focus of most experiments was to measure the time-mean flow fields and turbulent stresses, and expose some of the interesting characteristics of swirling jets. Only recently have researchers begun to pay more attention to the role played by underlying vortical flow structures and their dynamical evolution, e.g. Panda & McLaughlin (1994), Kurosaka *et al.*(2003) and the LadyHx group at the Ecole Polytechnique, Billant, Chomaz & Huerre (1998), Loiseleux & Chomaz (2003) and Gallaire & Chomaz (2003*c*).

Escudier, Bornstein & Maxworthy (1982) presented arguments, based on their experimental observations that, there is a clear separation of the roles of flow criticality and flow stability. It was proposed that the location of breakdown in the flow can be predicted by the transition from a super-critical to a sub-critical state to form an axisymmetric bubble, as in Benjamin (1962) for example. When this solitary wave or bubble reaches a certain critical amplitude, the wake-like velocity profile created in its interior becomes unstable to a discrete spectrum of spiral disturbances which grow rapidly, and it is these disturbances that are responsible for the appearance of a breakdown dominated by spiral waves. This point of view and its extensions (see below) has been supported recently by the computations of Ruith *et al.* (2003) and the experiments of LM.

During the past two decades, concepts of convective (CI)/absolute (AI), local/global and linear/nonlinear instabilities in open shear flows have been established by Fuchs, Ko & Bers (1981), Koch (1985), Chomaz, Huerre & Redekopp (1988), Monkewitz (1988), Huerre & Monkewitz (1990), Pier, Huerre & Chomaz (2001), Pier & Huerre (2001) and Huerre (2001), among many, and applied to swirling jet/wake shear-layers, e.g., Martin & Meiburg (1994), Delbende, Chomaz & Huerre (1998), Loiseleux, Chomaz & Huerre (1998), Lim & Redekopp (1998), Loiseleux, Delbende & Huerre (2000), Gallaire & Chomaz (2003*a b*) and Ruith *et al.* (2003). It appears, based on the major differences that have been observed, that one can probably divide these studies into two groups depending on subtle differences in the inlet velocity profiles. Some used inlet profiles with axial and azimuthal shear layers that intimately overlapped at a radius close to or coincident with the edge of the inlet, e.g. Martin & Meiburg (1994), Lim & Redekopp

(1998), Loiseleux, Delbende & Huerre (2000), Gallaire & Chomaz (2003*a*), Ruith *et al.* (2003) and also the present experiments. The most unstable modes observed by this group were more-or-less aligned with the local mean vortex line which implied that their instability mechanism was more of the K–H type and that even though the flow was nominally centrifugally unstable this mechanism did not play a major role in choosing the observed stability modes. AI was found to be significantly enhanced by the presence of the swirl in linear instability analysis of shear layers in centrifugally stable and unstable jets and wakes. The second major group considered inlet velocity profiles with the peak azimuthal vorticity in the axial shear layer, due to the axial flow, somewhat displaced from the location of the maximum axial vorticity in the azimuthal shear layer, due to the swirl flow. For example, in the studies of Gallaire & Chomaz (2003*b*), Billant *et al.* (1998) and Loiseleux & Chomaz (2003), the axial shear layer instability covered the range from approximately $r = 0.9R$ to $1.1R$ while the major part of the azimuthal shear layer covered the approximate range from $r = 0.5R$ to $1.1R$. In this case an intermittently co-rotating, co-winding helical wave $m = -2$ was found to be the most unstable. Thus, even though the mean vortex lines were counter-winding the instability waves did not follow the vortex lines and were dominated by the effect of the centrifugal instability, in contra-distinction to the cases above. This is similar to phenomena observed in Taylor-Couette flow with axial flow where the centrifugally induced pressure gradient is able to stretch, bend and reorient the mean vortex lines (Ludwieg 1961, 1964).

The objectives of the present research are to study the basic phenomenon of swirling jets, over a wide range of swirl number, S, with moderate values of Reynolds number, Re, and extending it to the case where the surroundings are also rotating. By using high resolution and real-time Digital Particle Image Velocimetry (DPIV), the velocity and vorticity fields have been precisely measured both on a central, vertical section of the jet and on horizontal slices at axial locations from the nozzle exit. Quantitative studies of the instabilities can be found in Liang (2003) (hereafter L) and LM.

2. Experimental set-up and procedures

2.1. *Apparatus*

An experimental program was designed which could cover the range of conditions of interest. This was accomplished in the apparatus shown as an assembly drawing in figure 1. It consisted of a vertical, swirling jet emerging into a large test tank which could be stationary or rotated independently. The working medium was water. More details about the assembly can be found in L and LM.

The swirling jet ended in a smooth nozzle attached to the inner cylinder. Contracting nozzles have been used in most experiments to produce a laminar and uniform non-swirling jet. However experiments have also shown that the fully developed swirling jets coming from a contracting nozzle, see e.g. Billant *et al.* (1998), had a central over-shoot in the axial velocity within the vortex core. Under these circumstances the inflow condition was hard to control since each rotation rate gave a different axial velocity profile. Thus a smooth and non-contracting nozzle of diameter $D = 1.5$ inch was used in the present experiments, even though it caused some slight non-uniformity and a higher level of turbulence in the exit flow.

The test tank was a large, transparent cylinder. A square tank surrounded the cylindrical tank and was filled with water to eliminate optical distortion. Both tanks were concentric with the upper nozzle assembly. The rotating element was designed to produce a jet with an initially uniform axial velocity and solid-body swirl or azimuthal

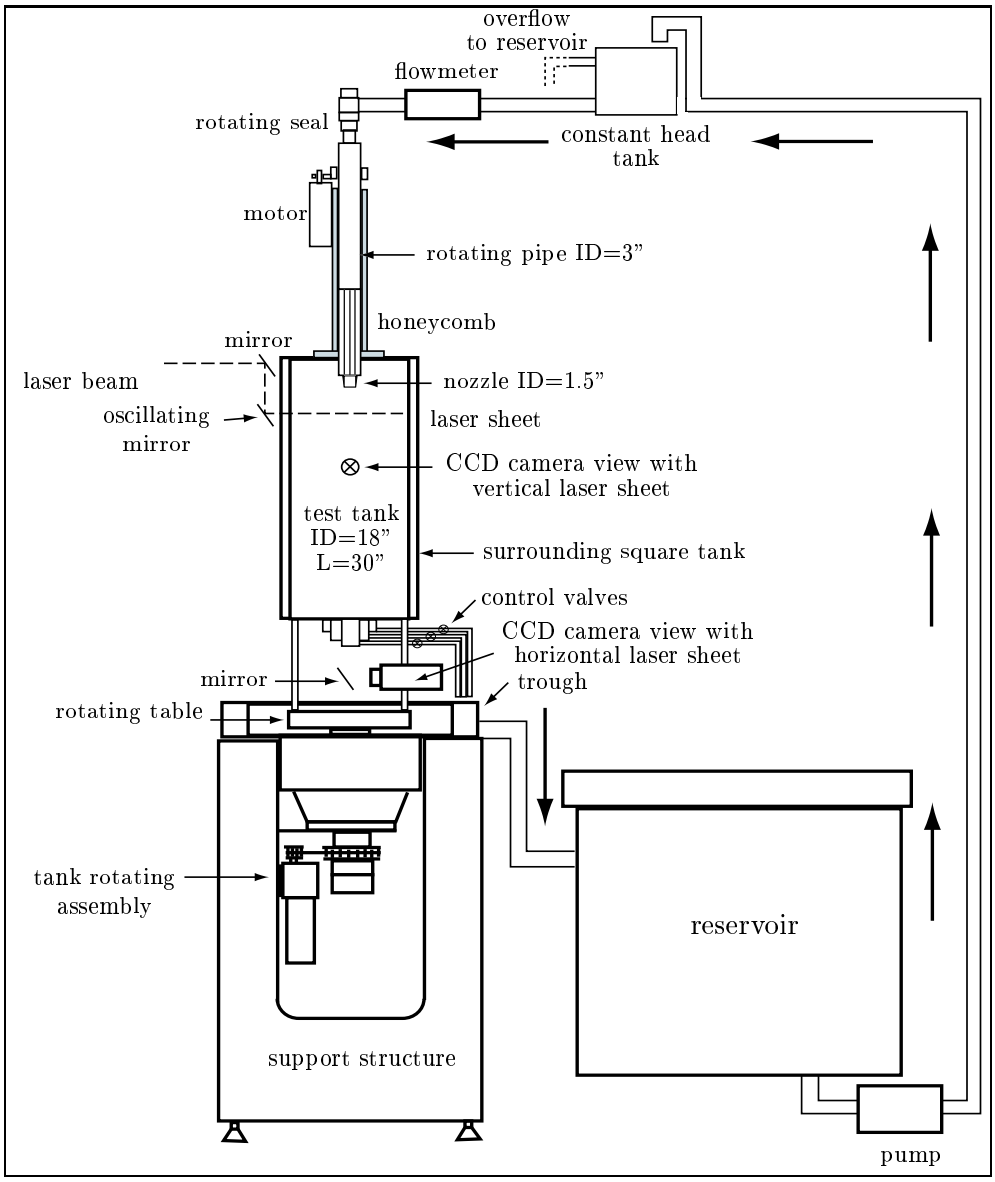

FIGURE 1. Sketch of the experiment set-up with the test tank stationary or rotating.

velocity, both with outer shear-layers to bring the velocity to that of the outer flow, i.e., the flow was centrifugally unstable by design. For cases with the test tank rotating, it was rotated for half an hour before the jet was started. In these cases, the jets in a counter-swirling tank were centrifugally unstable, while jets in the co-swirling tank could be either centrifugally stable or slightly unstable.

2.2. *Control parameters*

There are three independent control values for the swirling jet, flow rate, rotation rate of the nozzle and rotation rate of the test tank, which can be expressed in terms of non-dimensional parameters, Reynolds number Re, swirl numbers S for the jet and S_a

for the ambient. The Reynolds number is defined as

$$Re = UD/\nu \tag{2.1}$$

where the mean mass axial velocity, $U = Q/\pi R^2$, is the flow rate divided by cross-area of the nozzle exit, while D is the diameter of the nozzle exit, R is the radius of the nozzle exit, $D/2$, and ν is the coefficient of kinematic viscosity of water. The swirl number is defined as the ratio of the azimuthal velocity at the nozzle exit to U (also known as the Taylor or inverse Rossby number), i.e.

$$S = \Omega R/U \tag{2.2}$$

$$S_a = \Omega_a R/U \tag{2.3}$$

Here Ω and Ω_a s^{-1} are rotation rates of the nozzle and the test tank respectively. With the reservoir stationary, a moderate Reynolds number, $Re = 1000 \pm 50$, i.e. $U = 2.60$–2.88 $\mathrm{cm\,s}^{-1}$, was chosen for most studies, and a broad range of swirl number, $S = 0$ to 1.1, was covered to observe the phenomena of interest, e.g. vortex shedding, pairing, spiralling and breakdown. With the reservoir co- or counter-rotating with $S_a = \pm 0.35$, ± 0.51 and ± 0.70, a quantitative visalization study of the mean flow was carried out at $Re = 1000$ and 2000 with $S = 0$ to 1.3.

2.3. *Instrumentation*

In our laboratory a high resolution DPIV system has been developed, called Correlation Image Velocimetry (CIV) by Fincham & Spedding (1997). By using a series of sophisticated checking routines and by optimizing the particle size, time between frames, search area and correlation boxes, it is possible to obtain velocity vectors accurate to approximately 1% and vorticity to approximately 3% using a video based system with a standard 768×484 CCD array operating at the maximum of 30 frame s^{-1}. From these data velocity profiles, velocity vectors, circulation, vorticity contours, etc could be calculated and displayed.

Using CIV coupled with flow visualization it was possible to observe the geometry and detailed velocity and vorticity structures of instability waves. The light source was a 5 Watt Argon-ion laser. The laser sheet was made by a Function-generator-controlled mirror continuously oscillating at 200 Hz, which provided an effectively instantaneous pulse containing a high frequency scan. By changing the oscillation direction of the mirror, a laser sheet perpendicular to the axis of the jet or a sheet that contains the jet axis could be obtained as shown in figure 1. By introducing fluorescein into the jet from the top of the nozzle assembly, analog information could also be captured by video or still cameras. More detail is given in L and LM.

2.4. *Calculation of flow velocity from CIV data*

Time averaged flow fields in horizontal slices were assumed to be axisymmetric because of the circular geometry of the jet and the test tank. For example when calculating the instantaneous circulation on horizontal slices of the jet, integration around a circle at each radius was performed, i.e.

$$\Gamma = wr = \int_0^{2\pi} w(x, r, \theta) r \mathrm{d}\theta = \sum_{k=0}^{K-1} w(x, r, k\Delta\theta) r \Delta\theta$$

where $\Delta\theta = 2\pi/K$. Values are non-dimensionalized using: axial distance from the nozzle exit $= x/D$, radius $= r/R$, axial velocity $= u/U$, radial velocity $= v/U$, circulation

$= \Gamma/(2\pi\Omega R^2)$ and azimuthal velocity $= w/(\Omega R)$, where $\boldsymbol{u} = (u, v, w)$ in the cylindrical coordinate system (x, r, θ).

To obtain time-averaging flow fields using vertical or horizontal slices of the jet, 120 flow field realizations, $N = 120$, were used with the time step $\Delta t \approx 0.4\,\mathrm{s}$ between them. The sampling rate, $1/0.4\,\mathrm{s}^{-1}$, was about ten times faster than the rotation rate of the nozzle when $S = 1$ and $Re = 1000$, $\Omega = 1/4.38$ revolution s^{-1}, and the recording time, 48 s, covered about eleven full revolutions under this condition. Again using the circulation as an example, the time averaged mean quantity is then given by

$$\overline{\Gamma} = \frac{1}{T}\int_0^T \Gamma(t)\mathrm{d}t = \frac{1}{N}\sum_{n=0}^{N-1}\Gamma(n)\Delta t$$

with the root-mean-square (RMS) value of the corresponding fluctuation defined as

$$\Gamma' = \left(\overline{[\Gamma(t) - \overline{\Gamma}]^2}\right)^{1/2} = \left(\frac{1}{N-1}\sum_{n=0}^{N-1}[\Gamma(n) - \overline{\Gamma}]^2\right)^{1/2}$$

The vorticity of was calculated from the instantaneous axial and radial velocities on a vertical slice of the jets as:

$$\omega_\theta(x, r) = \frac{\partial u}{\partial r} - \frac{\partial v}{\partial x} = \frac{u(x, r) - u(x, r - \Delta r)}{\Delta r} - \frac{v(x, r) - v(x - \Delta x, r)}{\Delta x}$$

where Δx and Δr are the axial and radial spatial step of the meshed velocity fields calculated by CIV.

3. Observations

3.1. *Flow Visualization with* $\Omega_a = 0$

The following sections present flow visualisation studies of swirling jets with the test tank stationary.

For most studies, a moderate Reynolds number $Re = 1000$ was chosen with a wide range of swirl number $S = 0$–1.1 to cover four regimes: non-swirling jet with $S = 0$, weakly swirling jets in the range $0 < S < S_{c1} = 0.6$, strongly swirling jets before vortex breakdown with $S_{c1} < S < S_{c2} = 0.88$, and stable vortex breakdown for $S > 0.88$. Experimental phenomena under different conditions were demonstrated by (1) photographs of vertical and horizontal cross-sections (figures 2 and 3) illuminated by laser-induced fluorescein; (2) and instantaneous velocity vector images calculated from DPIV (figure 6). In figure 2, flows at $Re = 600$, 1000 and 2000 are shown together for comparison. Generally, the flow was more turbulent at higher Reynolds number for both non-swirling and swirling jets. Since no obvious difference in the flow criticality and instability has been observed for these three Re, further study and discussion concentrated on jets at $Re = 1000$.

3.1.1. *Non-swirling jets,* $S = 0$

Without swirl ($\Omega = 0$, i.e. $S = 0$), the jet evolved downstream, while the Kelvin–Helmholtz instability, resulting from the axial velocity difference between the jet and the ambient fluid, led to the tendency for the laminar shear-layer shed from the nozzle exit to roll up into discrete and axisymmetric vortex rings at $x \approx 2D$ (figure 2*a*). These vortex rings grew in the streamwise direction while propagating with a velocity of approximately one half of the mean flow, and resulted in the spreading of the jet. Vortex pairing was

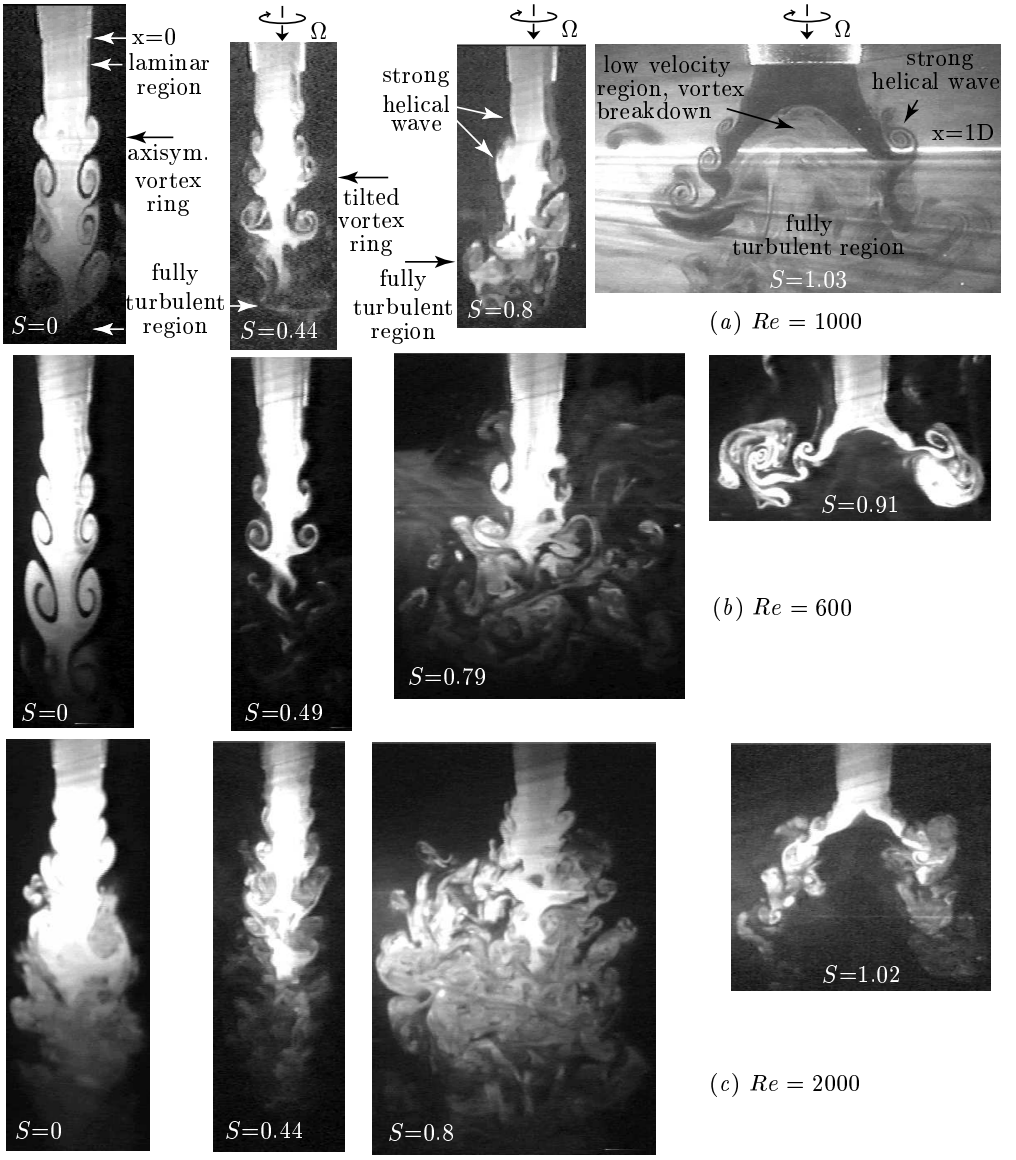

FIGURE 2. Instantaneous photographs with laser sheet illumination of a central, vertical slice of the jets, (*a*) $Re = 1000$, (*b*) $Re = 600$, (*c*) $Re = 2000$.

observed far downstream and accounted for most of the spreading of the jet (see e.g. Browand & Laufer 1975). The local vortex shedding frequency decreased axially until $x \geqslant 5D$, where the flow reached a fully turbulent state downstream and distinct vortices could no longer be observed .

3.1.2. *Weakly swirling jets,* $0 < S < S_{c1}$

With Re fixed and the swirl rate increasing slowly from zero, streaklines of the jet became helical due to the solid body rotation of the flow. The rotation direction of the mean flow was from right hand side to left on the vertical slice of the jet in figure 2 (*b–d*), and clockwise on horizontal slices shown in figure 3 (*a–d*) if viewed from the mirror in-

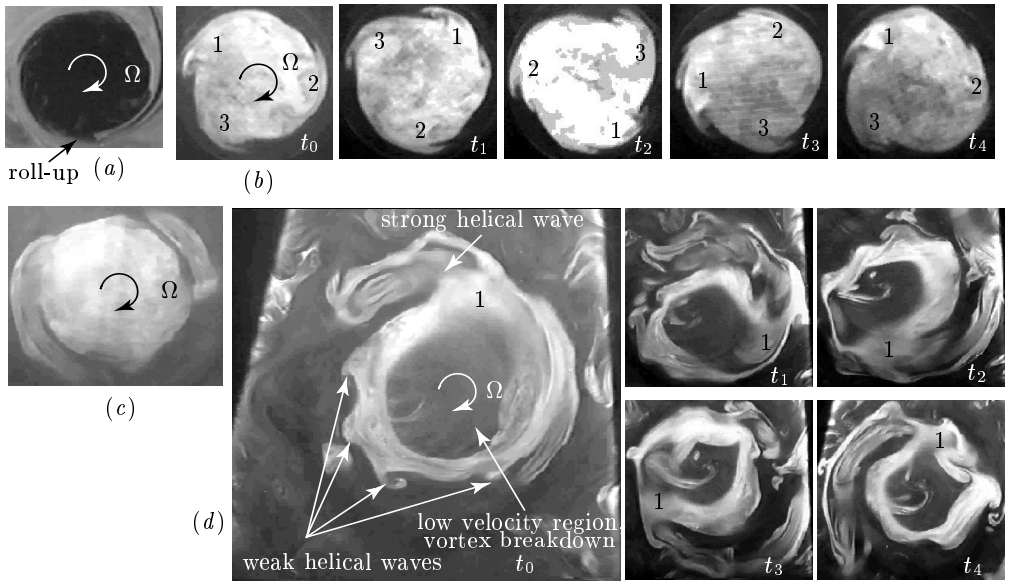

FIGURE 3. Instantaneous photographs of a horizontal slice of the jets, (*a*) $S = 0.44$ at $x = 1$D, (*b*) $S = 0.63$ at $x = 0.5$D, (*c*) $S = 1$ at $x = 0.5$D, (*d*) $S = 0.90$ at $x = 1$D. $Re = 1000$. In (*b*) and (*d*), the trace of helical waves, marked as '1', '2' and '3', is shown in one revolution, e.g. $t_0 = 0$, $t_1 = 0.25T$, $t_2 = 0.5T$, $t_3 = 0.75T$ and $t_4 = T$, where T is the time that the nozzle rotated one full turn.

stalled underneath the test tank. Vortex rings maintained their axial symmetry upstream and became tilted downstream. A secondary azimuthal shear-layer instability evolved between the rotating jet and the stationary ambient fluid. This type of vortex rolled up in a direction opposite to that of the solid body rotation, while it co-rotated with the jet (figure 3*a*, but for better idea of their structure and evolution, see figure 3*b* and *d* at larger S). These instability vortices, which had the appearance of helical waves, were only visible in horizontal cross-sections and were rapidly convected away by the mean flow.

In this regime, the axial shear-layer instability led to vortex rings that still dominated the flow, and vortices due to the azimuthal shear-layer were considered to be secondary. Small scale random turbulence grew in the shear-layer and made the flow visibly more turbulent than the non-swirling jet. The jet spread faster than a non-swirling one, and the entrainment of ambient fluid was higher (figure 3*a, b*). The laminar region became shorter at larger swirl number, and the fully turbulent region was located further upstream, e.g. at $x \approx 3D$ for $S = 0.44$.

3.1.3. *Strongly swirling jets,* $S_{c1} < S < S_{c2}$

As S increased further, the flow became more complicated and irregular (figure 2*c*), and vortices associated with instability of the azimuthal shear-layer grew stronger (figure 3*b*). When S was above the first critical value, i.e. $S_{c1} \approx 0.60$, the shear-layer lost its axial symmetry and helical waves with $m = +2$ or $+3$ grew and replaced vortex rings to become the dominant vortex structure. These strong, helical waves co-rotated with the mean swirl, with a phase speed that was the same as the rotation rate of the nozzle, both in direction and absolute value. Images at five instants with $\delta t = 0.25T$ apart during one revolution, T, were shown for case $S = 0.63$ in figure 3(*b*).

The break up of the flow symmetry, the existence and evolution of intense vortex

spirals, were detected first from a study of the azimuthal vorticity contours calculated from the velocity field on the vertical cross-section of the jets (see § 3.2.1). Then they were confirmed by careful observation of the dyed jet. More details can be found in § 3.2 and L. The vortex core was relatively stable and laminar close to the nozzle exit, e.g. at $x \leqslant 1D$ for $S = 0.80$ (figure 3*c*). After that, the flow rapidly became fully turbulent at $x \geqslant 2D$. At the same time, small scale vortices, e.g. random turbulence and weak helical waves, grew and made the larger scale vortices irregular and unorganized. This competition and interaction of instabilities made the vortex spiral very unstable and hard to visualize, especially as the flow approached the condition of vortex breakdown.

3.1.4. *Vortex breakdown, $S > S_{c2}$*

Vortex breakdown has been defined as an abrupt flow transition with a free stagnation point or region on the axis followed by a reverse flow and a fully turbulent region (figures 2*d* and 3*d*). The critical swirl number for breakdown to appear and stabilize in the flow is $S_{c2} = 0.88$ at $Re = 1000$ in the present experiments. In the range $S = 0.86$–0.88, vortex breakdown was unsteady and oscillated axially over a fairly wide range of amplitude (see § 3.1.5). After the structure of vortex breakdown stabilized, the flow became regular with fewer small scale vortices in the shear-layer. The vortex breakdown in the vortex core and strong helical waves in the shear-layer were well defined and clearly visible. After breakdown, the jet spread much faster and produced a high entrainment rate of ambient fluid. This highly mixed region moved closer to the nozzle exit as S increased further.

3.1.5. *Spacial-temporal variation of the stagnation point and the intermittancy of breakdown*

With Re fixed at 1000, for $S < 0.84$ no breakdown bubble appeared in the camera field of view, $0 < x < 4D$, during a long time observation. For $S > 0.88$ the bubble was always present and stabilized at some axial location, oscillating with a small amplitude along the axis. During the transition, i.e. $0.84 \leqslant S \leqslant 0.88$, a bubble repeatedly disappeared and appeared. Compared with the steady breakdown, this kind of unstable structure was highly turbulent and unsteady. As shown in figure 4, taken from many velocity vector plots, the stagnation point oscillated with large amplitude in this interval and no mean value could be meaningfully defined. Results at the stable end-states are given for comparison. High frequency fluctuations in the stagnation point location have been filtered by smoothing the profile.

The corresponding averaged axial location of stagnation points during one appearance of breakdown, $\overline{x}_{sp}$, is shown in figure 5(*a*). This average was done during the whole observation period for unstable breakdown, $0.827 \leqslant S \leqslant 0.876$, but was calculated after the initial transition period, i.e. during t_2, for stable breakdown with $S \geqslant 0.88$. The intermittancy calculated from long time analog-video observation is shown in figure 5 (*b*). Here the observation was made over the whole the tank during a typical two-hour taping for each condition, and I was calculated as the sum of the duration of each appearance of breakdown within the viewing area T_i, divided by the total observation time of two hours, i.e.

$$I = \sum_i T_i / 2hours$$

Normally, the swirl rate was increased gradually from $S = 0$. Only when investigating the hysteresis phenomenon (dashed line in figure 5 *b*), was the swirl number continuously decreased from a stable breakdown status, e.g. at $S = 1$. Under these two different initial conditions, the critical swirl rates at which the bubble the first appeared, $S = 0.86$ and

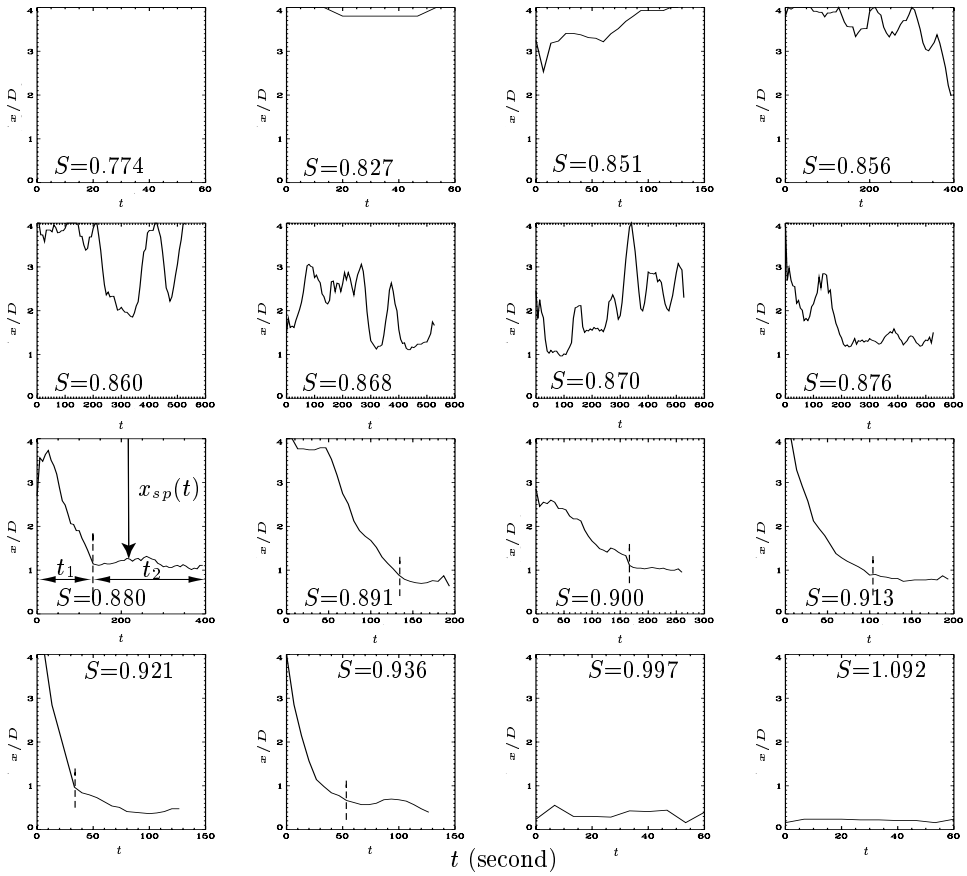

FIGURE 4. Time variation of the location for stagnation points along axis for various swirl numbers $S = 0.774$ to 1.092, $Re = 1000$. For stable breakdown with $S \geqslant S_{c2} = 0.88$, t_1 is the initial transition period before the steady state t_2.

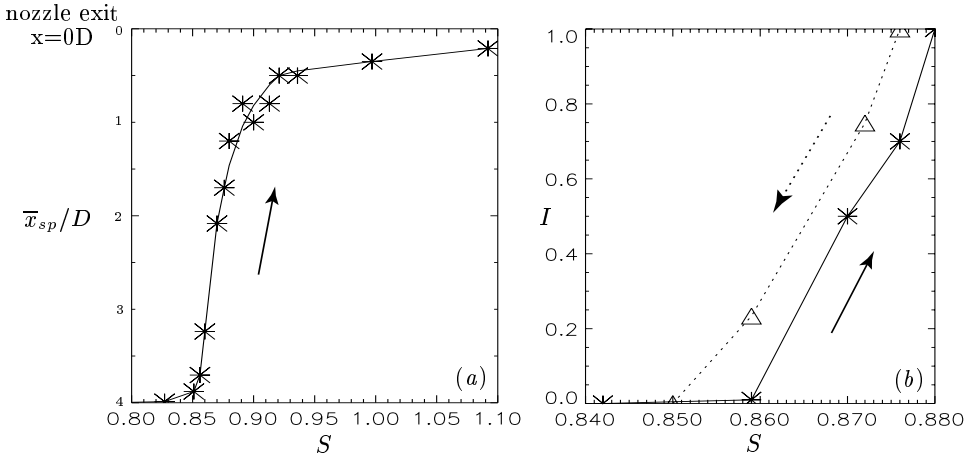

FIGURE 5. (a) The averaged axial location of stagnation points during one appearance of breakdown, $\overline{x}_{sp}$, calculated from figure 4. (b) Intermittancy of the appearance of vortex breakdown, I, based on long time data collecting with hysteresis phenomenon, solid line: S increased from 0, dashed line: hysteresis phenomenon as S deceased from 1. $Re = 1000$.

the first time the bubble did not appear after its disappearance, $S = 0.85$, are different and the former is larger, as expected.

3.2. *Vortex spiral morphology*

3.2.1. *Definitions*

In this introductory section, the definitions of various terms and symbols to be used are given for clarity. Following Martin & Meiburg (1994), the phase function of the disturbance at a fixed time is defined as $(kx + m\theta)$, k positive, where x is in the direction of the mean axial flow and θ increases in the direction of the basic rotation. Thus a mode with m positive $(+m)$ has a line of constant phase with a sense of winding in the opposite direction to the basic rotation and is called counter-winding, i.e., with increasing x a point on a line of constant phase moves in an azimuthal direction opposite that of the basic rotation. Conversely, a helix with m negative $(-m)$ has a sense of winding in the same direction as the rotation and is called co-winding. Additionally, the disturbance is said to be co-rotating if a point on a line of constant phase rotates in the same direction as the underlying rotation and counter-rotating if it rotates in the opposite direction. Also, one useful, physically based, way to discuss the results that follow is to note that in the present experiment the lines of constant phase and the finite-amplitude vortex structures that evolve are always more aligned with the mean vortex lines of the basic flow field (see § 6.2.2). This result is physically reasonable and is confirmed by some available theories, e.g., Martin & Meiburg (1994).

As mentioned previously all the unstable vortex spiral modes observed in the present experimental investigation co-rotated with the jet, and their phase speed was observed to be the same as the rotation rate of the nozzle, (see figure 3*b, d*). Their inclination, or their sense of winding, was in the direction opposite to that of the mean swirling flow, and more-or-less aligned with the local vortex lines, see § 6.2.2. In our present convention, these are designated at m positive modes. Figures 6 (*a*) and (*b*) show samples of the spatial evolution of vortices calculated from velocity/vorticity fields as $m = +3$ at $S = 0.78$ and $m = +2$ at $S = 1.03$, i.e. after vortex breakdown. Here for clarity, vortex spirals were reconstructed only in the outer shear-layer, and their angles, $tg^{-1}(-m/kr) = tg^{-1}(2\delta x/\pi\delta r)$, are marked at some axial locations. The number of spirals in the flow equalled the number of vortices that appeared at a fixed point on one side of the jet, during one revolution, on the vertical cross-section. Details concerning the temporal evolution of the spirals can be found in L and LM.

3.2.2. *The most unstable modes*

From the present investigation, the most unstable mode in the shear-layer was $m = 0$ for non-swirling and weakly swirling jets with $S < S_{c1} \approx 0.6$, where the large scale structure vortex rings dominated the shear-layer. When S increased over S_{c1}, vortex spirals/strong helical waves evolved and became the dominant vortex structure in the flow, and the most unstable modes were $m = +2$ or $+3$ before breakdown, i.e. $S_{c1} < S < S_{c2} = 0.88$. Good examples are shown in figure 6 (*a*) at $S = 0.78$ and figure 3 (*b*) at $S = 0.63$ from a horizontal cross-section $x = 0.5D$. After vortex breakdown $S \geqslant S_{c2}$, the spiral structure became regular and clearly visible. As vortex breakdown reached its steady state, spirals $m = +1$, $+2$ coexisted. For most cases, $m = +1$ was the most unstable one, i.e. had the larhest amplitude, and grew dramatically downstream of the stagnation region, e.g. in figure 3 (*d*) at $S = 0.9$ using a horizontal slice at $x = 1D$. Mode $m = +2$ was relatively strong upstream of the stagnation region even when the flow was dominated by $m = +1$ downstream. Examples are shown in figure 6 (*b*) at $S = 1.03$ and

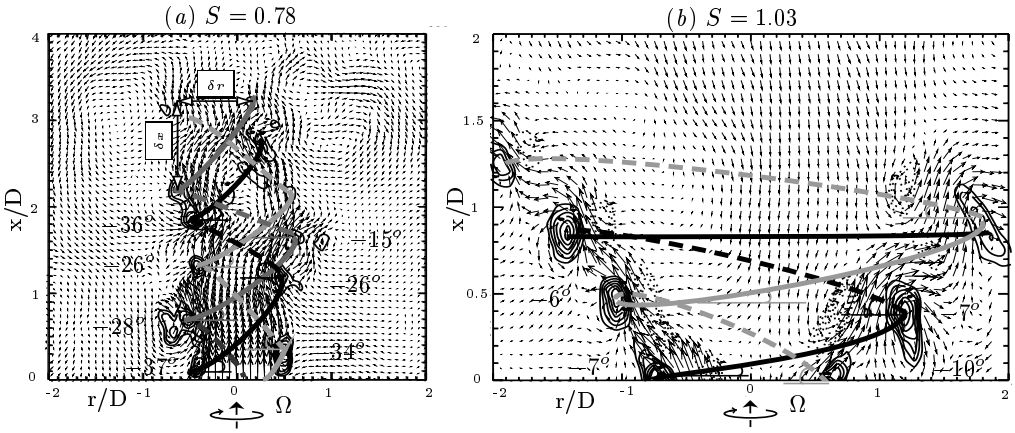

FIGURE 6. Spatial evolution of the vortex spirals, (*a*) $m = +3$ at $S = 0.78$ and (*b*) $m = +2$ at $S = 1.03$. $Re = 967$, i.e. $U = 2.65$ cm s^{-1}. Vortex spirals were reconstructed only in the outer shear-layer and marked as 'black', 'dark grey' and/or 'light grey'. The angle of these counter-winding helical waves is noted.

figure 3 (*c*) at $S = 1$ on the horizontal cross-section $x = 0.5D$. Weak helical waves can also be observed together with the strong vortex spiral $m = +1$ in figure 3 (*d*).

4. Quantitative flow measurements

In this section, time averaged flow fields of the swirling free-jet are shown on a vertical cross-section which contains the axis and covers the region $x = 0$–$4.5D$. For the horizontal cross-sections at different axial locations, $x = 0,\ 0.5,\ 1,\ 1.5,\ 2,\ 3D$ are considered. The Reynolds number was fixed at 967, i.e. $U = 2.65$ cm s^{-1}, and the swirl number ranged from 0 to 1.

4.1. *The axial velocity*

4.1.1. *Mean quantities*

The left column in figure 7 shows the radial distribution of the time mean axial velocity at each axial stations for various swirling numbers $S = 0,\ 0.44,\ 0.83,\ 0.91$. The amplitude of the mean axial velocity has been multiplied by 0.5 so that profiles with $0.5D$ axial distance between them would not overlap. The small over-shoot at the shoulder of the inflow is probably caused by the design of the nozzle, see LM. This over-shoot imposed a small wake-like defect on the inflow so that S_{c2} is slightly lower than when the profiles were flat (see details in L and LM).

Before vortex breakdown, the form of the axial velocity profile was basically a flat-top and became jet-like downstream, with the maximum velocity on the axis. For strong swirl rates $S \geqslant S_{c2}$, vortex breakdown appeared on the jet axis. Around and downstream of the stagnation region, the axial velocity maximum was displaced radially from the axis, and the basic profile became strongly wake-like, i.e. a region of reversed flow was found downstream of the stagnation point. The breakdown structure moved upstream as S increased further. At $S > 0.9$, the stagnation point was located so close to the nozzle exit that the axial velocity at $x = 0$ became of the wake type, i.e. the influence of the breakdown propagated into the nozzle. Based on these measurements it is possible to quantify the rapid radial spreading of the jet, especially in the neighbourhood of vortex breakdown. Details are given in L and LM.

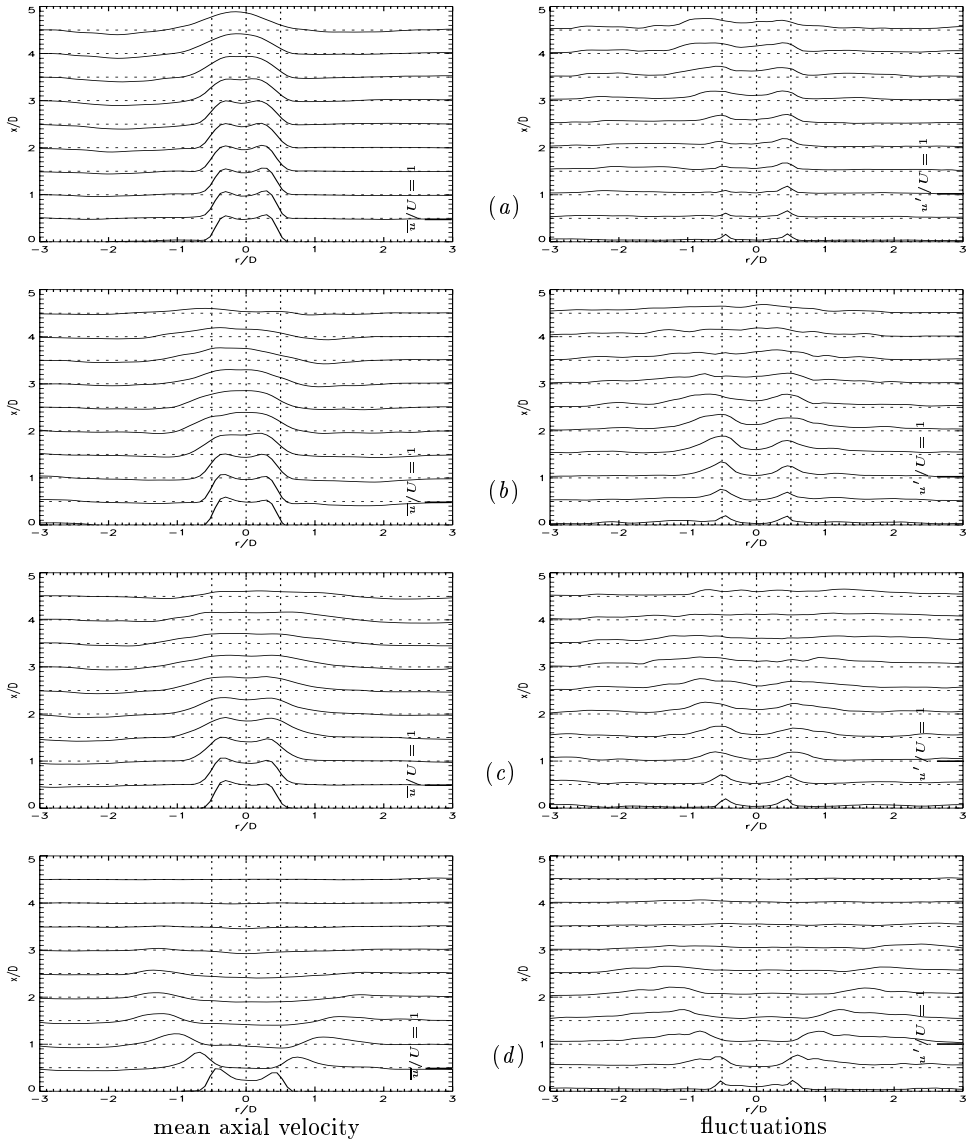

FIGURE 7. Left column: dimensionless mean axial velocity ($\times 0.5$) versus r/D, right column: dimensionless RMS fluctuated axial velocity versus r/D along axis, at (a) $S = 0$, (b) $S = 0.44$, (c) $S = 0.83$, (d) $S = 0.91$. $Re = 967$, i.e. $U = 2.65$ cm s^{-1}, $N = 120$, $\Delta t = 0.4$ s.

4.1.2. *RMS fluctuations*

The right column in figure 7 presents distributions of the dimensionless RMS value of the axial velocity fluctuation, for various swirl rates at $Re = 967$ from 120 realisations of the velocity field.

For all flows, upstream, e.g. $x \leqslant 3.5D$ for $S = 0$, $x \leqslant 2.5D$ for $S = 0.44$, $x \leqslant 2D$ for $S = 0.83$ and 0.91, the fluctuation distribution had maxima off the axis with high levels of turbulence in the shear-layer (both outer and inner shear-layers after breakdown), and a low-level of turbulence in the neighbourhood of the axis, i.e. in the vortex core and the bubble. The amplitude of turbulence increased and the highly turbulent region spread as S increased.

Before vortex breakdown, fluctuations downstream, e.g. $x > 3D$ for $S = 0.44$ and 0.83, were flat with high amplitude, while the turbulence level in the vortex core was comparable with that in the shear-layer. The flow became fully turbulent in this region. The rapid mixing of the fluid in the shear-layer and the vortex core was only observed in swirling jets, while the non-swirling jet reached its fully turbulent region far downstream, $x \geqslant 5D$. This fully turbulent region moved upstream and spread outwards and inwards as the swirl number increased.

After vortex breakdown, $S > S_{c2}$, the downstream area of the jet, for example $x > 2D$ for $S = 0.91$, contained weak turbulent and mean flow. The high fluctuation region was restricted to shear-layers surrounding the bubble. Turbulence in the reverse flow was relatively weak.

4.2. *The radial velocity*

4.2.1. *Mean component*

The left column in figure 8 shows the radial distribution of the time mean radial velocity at each axial station for various swirl number $S = 0,\ 0.37,\ 0.83,\ 0.91$ at $Re = 967$.

For all rotation rates before breakdown, the radial velocity was up to 10% of U within the shear-layer. Only for $S \geqslant S_{c2}$, was the amplitude of the mean radial velocity comparable with the other two components of velocity. This large mean value region was located upstream and within the spreading jet between inner and outer shear-layers.

4.2.2. *RMS fluctuations*

Before breakdown, even though the mean radial velocity was weak when compared with axial and azimuthal components, relatively high levels of turbulence appeared in the shear-layer and the fully turbulent region (right column in figure 8), which shows that turbulence was always three dimensional. After breakdown, it should be noted that the highly turbulent region spread more outwards in the radial velocity distribution than in the axial velocity distribution, and the maximum was located at the outside shear-layer, which was centrifugally unstable. This mismatch of the high fluctuation region also existed between the axial and the azimuthal velocities with the azimuthal shear-layer located slightly outwards than the axial shear (figure 13).

4.3. *The azimuthal velocity and circulation*

4.3.1. *Centrifugal instabilities*

Compared with the non-swirling jet, the additional presence of swirl can result in an unstable radial stratification of the angular momentum, which leads to the possibility of centrifugal instability. Rayleigh's (1888) inviscid criterion is a necessary and sufficient condition for instability for inviscid rotating flow. In the present experiments this inviscid criterion reduces to the statement that the azimuthal shear-layer is centrifugally unstable if the circulation decreases radially outward.

4.3.2. *Resolution of the peak circulation*

The theoretical profile of the circulation in the jet in solid body rotation as a function of radius, at $x = 0D$, is described by the solid line in figure 9 (*a*). It has a sharp peak at $r = R$ with a value of unity, after non-dimensionalization by $\Gamma_R = 2\pi\Omega R^2$. After the peak, the circulation drops immediately to zero. However, in practice, this result could not be realized for several reasons. The laser sheet could only be placed close to the nozzle exit, not right at it, in order to have enough particles to define the flow, and, more importantly, to exclude the intense reflection from the nozzle which degraded

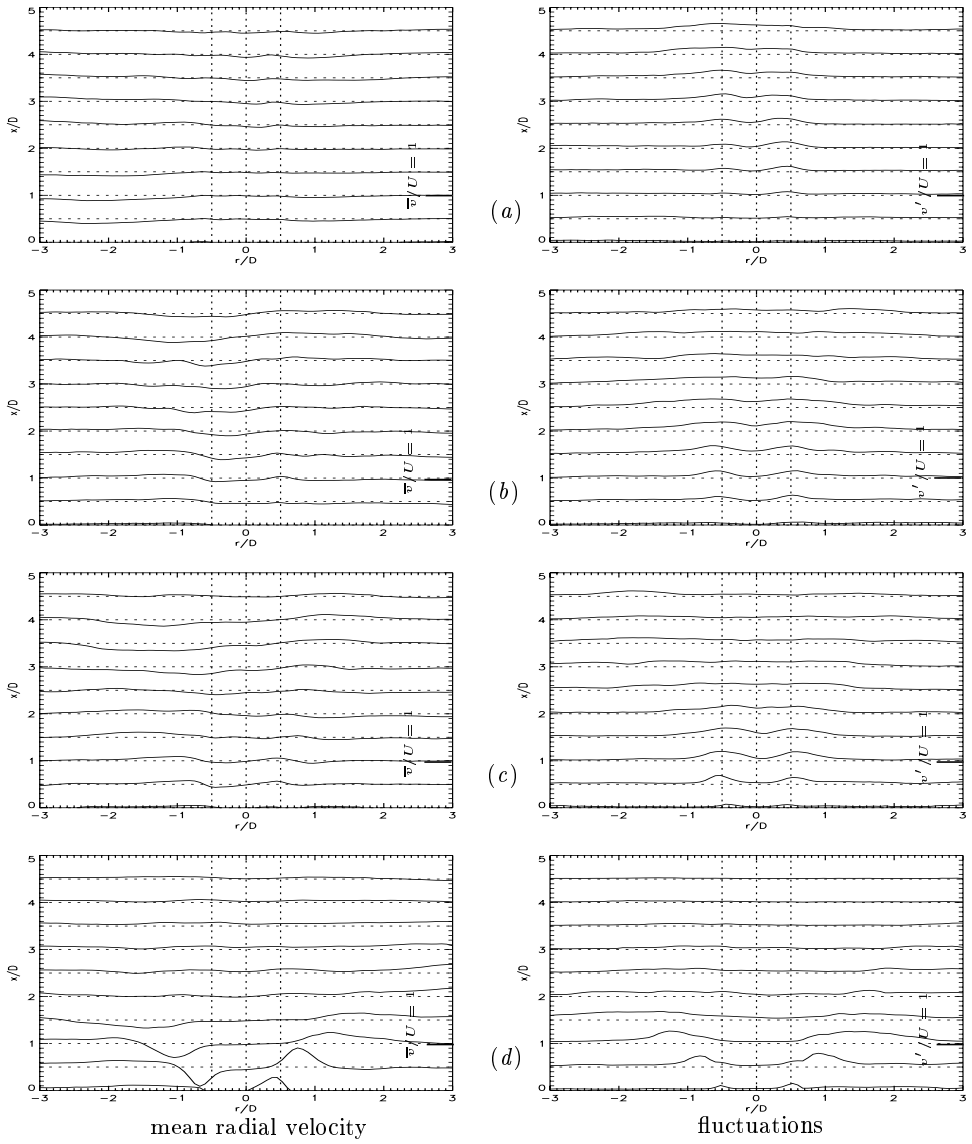

FIGURE 8. Left column: dimensionless mean radial velocity versus r/D, right column: dimensionless RMS fluctuated radial velocity versus r/D along the axis, at (a) $S = 0$, (b) $S = 0.37$, (c) $S = 0.83$, (d) $S = 0.91$. $Re = 967$, $N = 120$, $\Delta t = 0.4$ s.

the image. At this distance from the nozzle exit, no matter how short it was, the axial and azimuthal components of velocity had already diffused somewhat. Other technical limitations included: (1) the variable distance between the horizontal laser sheet and the CCD camera underneath the test tank. Thus the ability to zoom in was limited by the need to cover a large fraction of the flow field, not just a small portion. (2) the finite number of pixels of the CCD array used to capture the flow field. Thus as measured, the profile must be smooth and continuous and have a peak lower than unity. The measured profile is shown by the dashed line in figure 9 (a). These data were recorded at $x = 0$ with the highest possible resolution of our optical system.

The effect of the resolution of the optical system is demonstrated by the maximum

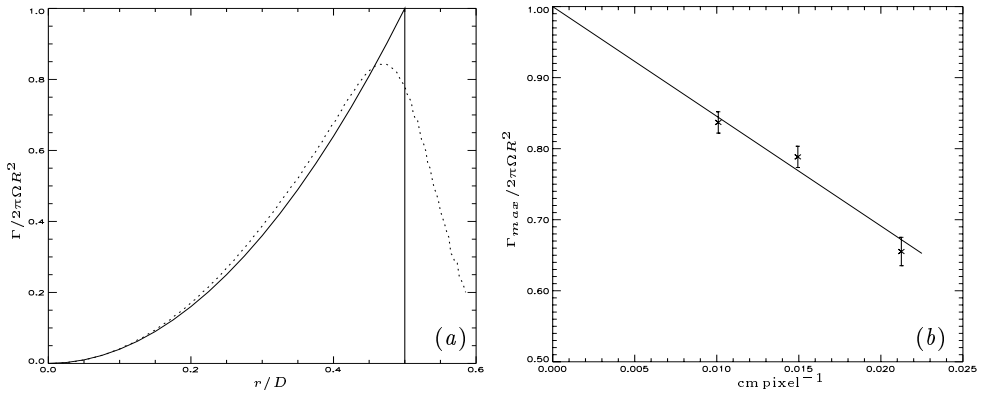

FIGURE 9. (*a*) The distribution of the dimensionless circulation of a solid body rotation at the nozzle exit $x = 0$. The solid line presents the theoretic profile, and the dashed line is calculated from our experiments at the best resolution. (*b*) Resolution of our optical system demonstrated by the maximum time averaged circulation at $x = 0$, $Re = 967$.

of the time mean circulation versus the image resolution (figure 9 *b*) in the horizontal cross-section located close to the nozzle exit. The resolution of the image is presented by the number of centimeters covered by a pixel in each image. The maximum of the normalized circulation that can be reached is 0.84 at $x = 0$ with the highest resolution of our optical system. At this maximum resolution, however, only a small portion of the flow field was covered. To cover a large enough area to collect meaningful velocity data, a smaller resolution had to be used. However, this was not believed to be a major problem, because the test case considered above was the most extreme possible and not representative of measurements further from the nozzle exit. Extrapolation of the line to 0 cm pixel^{-1}suggests that the maximum circulation could, in fact, be unity, but this is unlikely due to the evolution of the profile after the nozzle exit.

4.3.3. *Mean component*

Figures 10 show the spatial distribution of the time mean circulation at five axial stations, $x = 0,\ 0.5,\ 1,\ 1.5,\ 2D$ for $S = 0.38, 0.78, 0.91, 0.98$ at $Re = 967$. Profiles of the azimuthal velocity are similar in shape to the profiles of the circulation except for the location of maximum values. The gradient of the circulation decides whether the shear-layer is centrifugally stable or unstable, which is the critical information to be found from the measurement on the horizontal cross-sections of the jet. Thus in the following, the discussion is based on profiles of circulation, and the slight differences between locations of the two maxima are ignored.

For weakly swirling jets, say at $S = 0.38$, circulation profiles at axial locations relatively close to the nozzle, $x = 0$–$1.5D$, were similar and 'hill' shaped with the peak located at $r = 0.92R$. Downstream $x \geqslant 2D$, the circulation distribution became flat with a relatively low amplitude due to the spreading and decay of the jet. The flow maintained solid body rotation at small radii, and at large radii the circulation decreased and eventually dropped to zero. The jet flow could then be separated into two regions: the region before the maximum circulation is designated as the *vortex core*, and the area at larger radii is the *shear-layer*. At steady state, fluid of the test tank was forced by vorticity recirculation to slowly co-rotate with the jet but with a very much smaller angular velocity and momentum. The decrease in circulation in the azimuthal shear-layer satisfied the condition for centrifugal instability in all cases. The Kelvin–Helmholz instability of the combined azimuthal and axial shear-layers enhanced the mixing efficiency of the jet

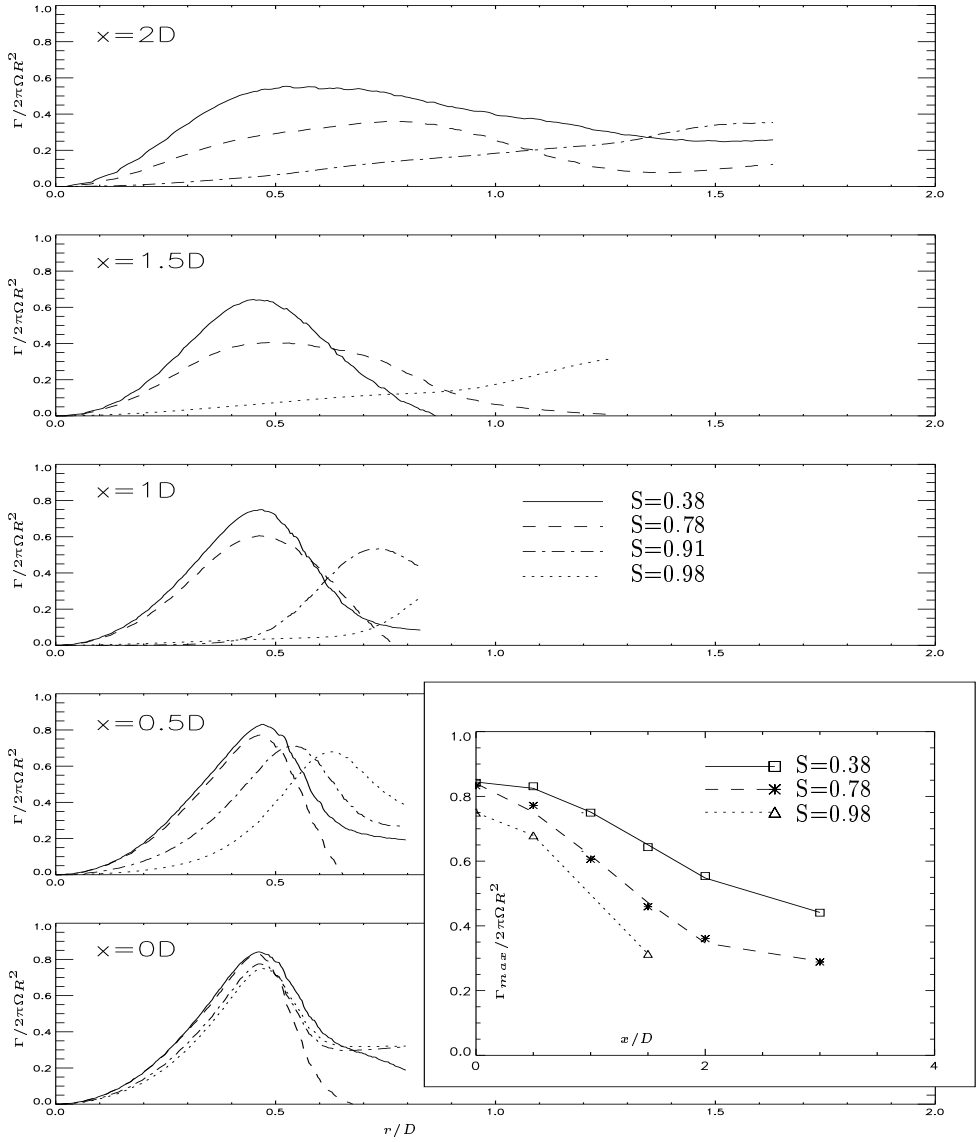

FIGURE 10. Dimensionless mean circulations versus r/D, for $S = 0.38,\ 0.78,\ 0.91,\ 0.98$, at axial locations $x = 0,\ 0.5,\ 1,\ 1.5,\ 2D$, and the axial decay of the maximum circulation. $Re = 967$.

with the ambient fluid, and the flow decayed faster than the non-swirling jet. Panda & McLaughlin (1994) argued that the centrifugal instability inhibits the K-H instability but causes higher entrainment. In our opinion, for weakly swirling jets, $S < S_{c1}$, the centrifugal instability enhanced the mixing but the K–H instability still appeared to dominate the flow. The solid body rotating region, i.e. vortex core, was relatively stable or less turbulent since it was centrifugal stable.

When the swirl number increased further to $S = 0.78$, the circulation distribution at $x = 0$ was similar to that for $S = 0.38$, with almost the same value of the peak and reached this peak at the same radial location. Away from the nozzle exit, the maximum of the circulation amplitude decayed faster for larger swirl number and the region of decreased circulation spread out rapidly.

After vortex breakdown, $S > S_{c2}$, the circulation distribution was still 'hill' like at $x = 0$, reaching its maximum at the same radial location as for swirling jets before breakdown. But the amplitude of the maximum was slightly lower. Away from the nozzle exit, the circulation not only decayed faster, but its maximum was relocated at a larger radial position. This displacement of the circulation maximum to a larger radius, as well as the displacement of the maximum of the axial velocity, is the signature of a vortex breakdown. At $x = 0.5D$, the circulation peaked at $r = 0.54D$ for $S = 0.91$ and at $r = 0.62D$ for $S = 0.98$, while it peaked at $r = 0.47D$ for $S = 0.38$ and 0.78. The stagnation region was located around $x = 0.5D$ for these two swirl numbers. At $x = 1D$, downstream of the stagnation region, the maximum circulation was located further away from the axis, to $r = 0.72D$ for $S = 0.91$, and out of the region of investigation for $S = 1$. In many ways it appeared as if the jet was flowing around an object inserted into the flow. Within the breakdown structure, the circulation amplitude was almost zero, indicating a very low angular momentum in this region. The region of non-zero circulation was spread out to $r \geqslant 1.5D$ at $x \geqslant 1.5D$ for $S = 0.91$ and 0.98.

The axial decay of the maximum circulation at various swirl rates is also shown in figure 10. As expected, the spatial decay was faster for larger swirl numbers. The decay was slower for the circulation than that for the azimuthal velocity, especially after breakdown, since the maximum azimuthal velocity was displaced to larger radii at larger swirling rates.

5. Preliminary study with $S_a \neq 0$

An investigation of swirling jets in a co- or counter-rotating test tank has also been carried out. This was originally designed as a way to study flows that could be either centrifugally stable or unstable, i.e., with S_a greater than S the flow would be centifugally stable while with S_a negative the flow would be even more unstable than the stationary case. Due to the technical difficulty of introducing the laser beam and recording data as the test tank rotated, up to now the study has been based on still images from flow visualizations of fluorescein dye. None-the-less, several interesting phenomena have been observed.

The first striking observation is that, non-swirling jets, with $S = 0$ in the frame of laboratory, behaved similarly whether the test tank was stationary, $S_a = 0$, or co- or counter-swirling, $S_a = \pm 0.35$ to ± 0.70 (e.g. figure 11 *a*). The mean flow/streamline evolved downstream with vortex rings rolling up and propagating. There was a clear observation of vortex breakdown when the test tank and nozzle rotated at the same rate with $S = S_a = 0.70$ (figure 11 *e*) in what was previously called, in LM, the strong rotation regime. Under this condition, the fluid in the tank and the exit jet were in a solid body rotation at the same rate and the only instability involved was K–H instability due to the axial velocity difference between the jet and its surrounding. For all swirl rates before breakdown, the flow seemed more turbulent in a counter-rotating ambient, e.g. compare jets with $S = 0.4$ and $S_a = \pm 0.7$ (figure 11 *b c*). But breakdown appeared earlier for flows in co-swirling surroundings, e.g. $S_{c2} = 0.7$ with $S_a = 0.7$ while $S_{c2} = 0.85$ with $S_a = -0.7$ (figure 11 *e f*).

Mean flow characteristics after breakdown, such as the criterion for breakdown and the axial distance between the stagnation point and the nozzle exit, were found to be strongly dependent on the absolute swirl number of the jet, S, rather than the swirl difference, $S - S_a$, or ratio between the jet and its ambient, S/S_a. The critical swirl number for breakdown S_{c2} was only slightly different in stationary and counter-swirl ambient but it was definately lower when the test tank co-rotated with the jet. For example, as shown

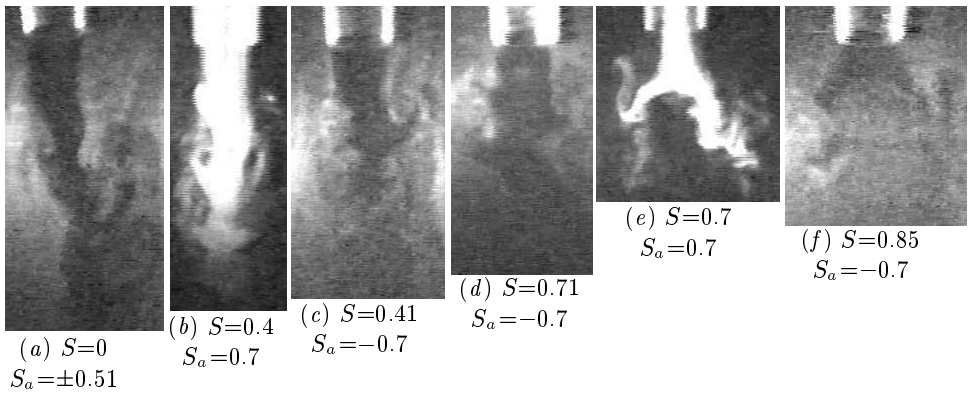

FIGURE 11. Instantaneous photographs with laser sheet illumination of a central vertical slice of the jets at (*a*) $S = 0$ and $S_a = \pm 0.51$, (*b*) $S = 0.4$ and $S_a = 0.7$, (*c*) $S = 0.41$ and $S_a = -0.7$, (*d*) $S = 0.71$ and $S_a = -0.7$, (*e*) $S = 0.7$ and $S_a = 0.7$, (*f*) $S = 0.7$, $S_a = 0.7$. $Re = 1000$. Note that here the photographs were taken of the rotating tank from the laboratory frame of reference and this accounts for the poorer image quality from figures 2 and 3.

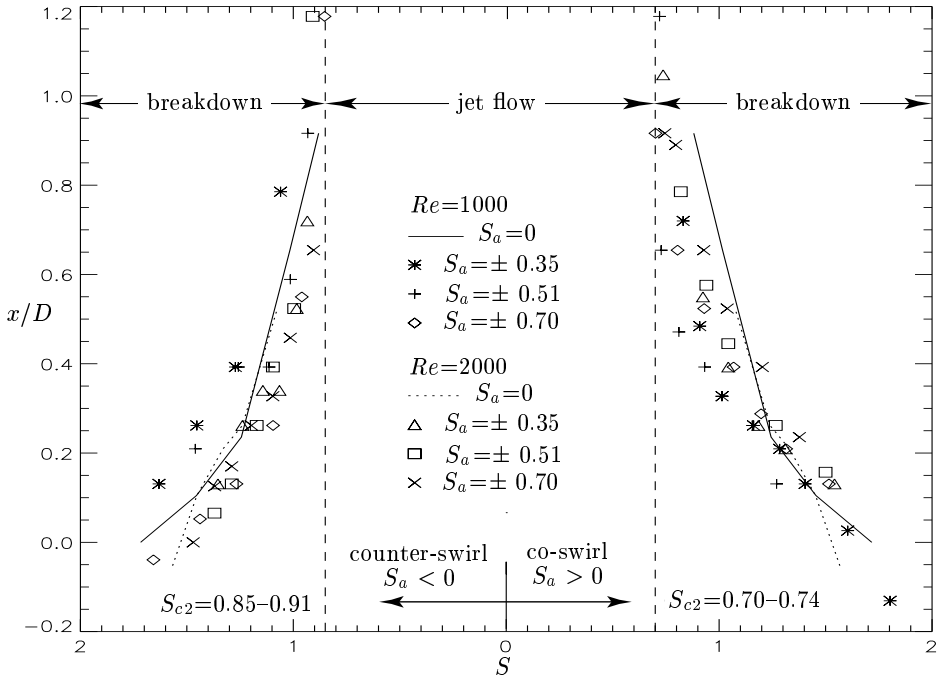

FIGURE 12. The axial location of stagnation points versus the swirl number of jets with the test tank stationary, i.e. $S_a = 0$ or rotating at $S_a = \pm$ 0.35, 0.51 and 0.70. $Re = 1000$ and 2000.

in figure 12, $S_{c2} \approx 0.85$ at $Re = 1000$ and 0.91 at $Re = 2000$ for non- and counter-rotating surroundings, and $S_{c2} \approx 0.70$ at $Re = 1000$ and 0.74 at $Re = 2000$ for co-swirling surroundings. This suggests that the mechanism of breakdown depends mainly on conditions in the vortex core, while instabilities, resulting from the swirl difference, have some but not a major effect. This observation provides further experimental support for suggestions given by Escudier *et al.* (1982) that there is clear separation between flow criticality and flow stability.

6. Conclusions and discussion

6.1. *Conclusions*

The characteristics of a swirling jet in both rotating and non- rotating surroundings has been studied in the present investigation. These include a complete discussion of the mean and turbulent velocity components, and their spatial distribution, the criteria for the appearance of steady vortex breakdown and its unsteady character at intermediate values of the swirl parameter.

K–H instability in the axial shear-layer, leading to vortex ring formation $m = 0$, dominated non-swirling and weakly swirling jets for $0 \leqslant S < S_{c1} = 0.6$. After the introduction of rotation, the combined axial/azimuthal shear-layer became unstable and co-rotating helical waves were produced. For weakly swirling jets, vortex rings maintained their axisymmetry upstream, and became tilted downstream. For strongly swirling jets before breakdown, i.e. $S_{c1} \leqslant S < S_{c2} = 0.88$, helical waves grew and replaced vortex rings to become the dominant vortex structure. The most unstable modes were $m = +2$ and $+3$. Many weak helical waves of other wave numbers and random turbulence made these vortex spirals irregular and unorganized. After vortex breakdown, small scale turbulence was suppressed and the large scale structures became well-organised and clearly visible. When vortex breakdown reached its steady state, strong helical waves $m = +1$ and $+2$ coexisted, with $m = +1$ having the largest amplitude. Here the helical modes co-rotated with the jet, while their inclination, or sense of winding, was in the direction opposite to that of the mean flow. The mean axial velocity profile was jet-like for flows before vortex breakdown and became wake-like after breakdown.

The effect of rotating the surrounding fluid was to slightly decrease the critical value of breakdown S_{c2} when the outer tank was co-rotating and to leave it unchanged when counter-rotating.

6.2. *Discussion*

6.2.1. *Criteria for breakdown*

Based on experimental, theoretical and numerical studies, Spall, Gatski & Grosh (1987) proposed a criterion for the onset of symmetric vortex breakdown, that the Rossby number Ro (or inverse swirl ratio) satisfied:

$$Ro = u(r^*, x_0)/(r^*\Omega) \leqslant Ro_c = 0.65 \tag{6.1}$$

for $Re \geqslant 100$. Where u is the axial velocity, r^* the radius of the maximum of the swirl velocity w, x_0 the axial location far upstream from the stagnation point, and Ω the core rotation rate near the vortex centerline $r = 0$. Based on previous theories and experiments, Billant *et al.* (1998) provided another criterion:

$$Si = \Big(\int_0^\infty \frac{w^2(r, x_0)}{r} dr\Big)^{1/2} / u(0, x_0) \geqslant Si_c = 0.707 \tag{6.2}$$

and found a good agreement with their experiments for different Reynolds numbers and two nozzle diameters, $D_1 = 4\,\mathrm{cm}$ and $D_2 = 2.5\,\mathrm{cm}$. In their work, Sp was defined, from the measured velocity profiles, as

$$Sp = \frac{2w(0.5R, 25\,mm)}{u(0, 25\,mm)}$$

with $Sp_c = 1.41$, i.e. $Si_c \approx 0.5 Sp_c = 0.705$ for breakdown. The critical Rossby number was calculated to be $Ro_c = 0.51$–0.65 for D_1 and $Ro_c = 0.80$–0.84 for D_2.

In the present experiments, breakdown was found well downstream of the nozzle and

oscillated axially for $S = 0.84$–0.86. At larger swirl rate, i.e. $S \geqslant S_c = 0.88$, breakdown was stabilized further upstream, and its effect entered the nozzle exit and made the exit flow wake-like. The criteria (6.1) and (6.1) were calculated close to the nozzle exit, $x_0 = 3$–$5\,\mathrm{mm}$, to give $Ro = 0.69$, $S_i = 0.66$ for $S = 0.86$ and $Ro = 0.82$, $Si = 0.69$ at $S_{c2} = 0.88$. The critical swirl parameter of the present investigation, $Si_c = 0.69$ at $S_{c2} = 0.88$, agrees well with the value 0.707 proposed by Billant *et al.* (1998). The value of Si increased quickly for larger swirl rates as the bubble moved closer to the nozzle exit and caused $u(0, x_0)$ to decrease rapidly. The criterion based on the Rossby number only worked for the smaller swirl rate, at which condition, a symmetric yet unstable breakdown was occasionally formed downstream. $Ro = 0.69$ for $S = 0.86$ is quite close to the value 0.65 proposed for the onset of symmetric breakdown.

6.2.2. *The most unstable modes*

Agreements of the rotation phase speed/direction and the winding angle/direction of the most unstable helical modes have been found between some of former experiments and theories and the present investigation.

The phase speed of each unstable helical wave observed in the present experiments is the same as the rotation rate of the nozzle, both in direction and absolute value, both before and after breakdown. It should be noted that the rotation rate of the vortex core of the inlet flow is calculated to be exactly the same as that of the nozzle (see LM), the achievement of which was one of the major reasons for the present design. This phenomenon was first caught by observation of the vertical and horizontal slices (figures 2 and 3) of the flow. It was then confirmed in the power spectral study (L and LM), in which the spectra peak was very clearly at some multiple of the rotation rate of the nozzle, which were predicted as the most unstable modes from earlier analog observation. Support was found in two recently published/submitted experimental papers. In an investigations of a confined swirling flow by Kurosaka *et al.*(2003), an axisymmetric vortex breakdown bubble was most affected and transformed to a co-rotating spiral vortex breakdown with $m = +1$, shortly after the introduction of forcing with $m = +1$ and in a frequency range that corresponded to a rotation rate almost equal to that of the vortex core of the inlet flow. The second supporting paper was written by the LadHyX group, Gallaire & Chomaz (2003*c*), and is, as far as we are aware, presently under review. This further instability study used the same swirling free-jet as used by Billant *et al.*(1998) and Loiseleux *et al.*(2000). In the first published papers by this group, the natural rotation rate of the most unstable helical waves was found to be $1/3$ smaller than that of the vortex core of the inlet flow, but in this latest paper, they corrected the ratio $1/3$ to $1/10$. Assuming that this newly reported value of the ratio is more accurate and reliable, the forcing phase speed, which was used by them to achieve the most amplified helical waves, with $m = +2, +3$ before breakdown, was one order of magnitude, 10 times, greater than the natural value of $1/10$, i.e., the same as the rotation rate of the inlet vortex core. This agrees well with the present observation. Furthermore, using the very recent stability calculations of Gallaire & Chomaz (2003*b*), we find agreement that the calculated phase speed of their $m = +1$ and $+2$ modes in a temporal stability study is close to the rotation rate of the vortex core at the inlet. Of course, the velocity profiles used in the above experimental and numerical investigations are somewhat different from ours and the comparison is only suggestive and not absolute.

As for the winding direction and angle of the most unstable helical waves, firstly an attempt is made to try to put the present experimental results into some sort of theoretical framework. The one that seems to work well is contained in the early work of Howard & Gupta (1962) who gave a sufficient condition for the temporal instability

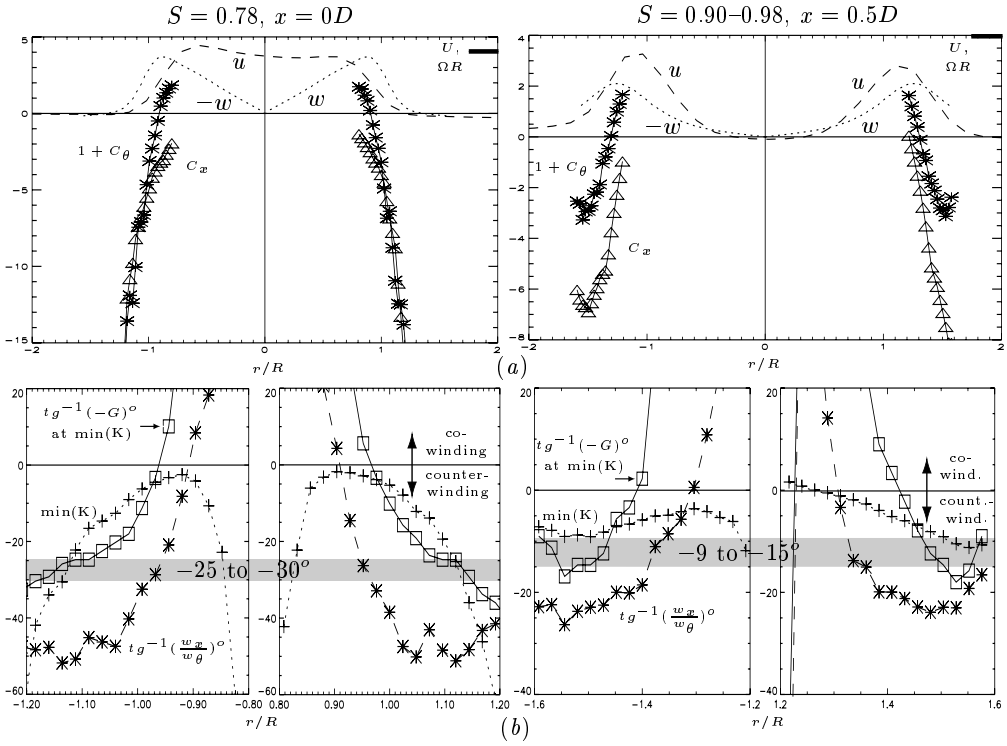

FIGURE 13. The angle of the most unstable wave within the outer shear layer at the inlet for strong swirling jet before breakdown and around the stagnation point for flow after breakdown. (a) velocity profiles (u_x, u_θ) and vorticity constants $(1+C_\theta, C_x)$. (b) minimum of (K_{HG}), the angle of the wave $tg^{-1}(-\frac{m}{kr})^{\,o}$ at $\min(K_{HG})$ and the angle of the mean vortex $tg^{-1}(-\frac{1+C_\theta}{C_x})^{\,o}$, K_{HG} defined by Howard & Gupta (1962).

of swirling flow. The condition is a function of $G = \frac{m}{kr}$, $C_x = \frac{r}{w}\frac{du}{dr}$ and $C_\theta = \frac{r}{w}\frac{dw}{dr}$,

$$K_{HG} = (1 + C_\theta) - GC_x - \frac{1}{8}[C_x + G(C_\theta - 1)]^2 \geqslant 0 \tag{6.3}$$

where (u, w) and $(\omega_x, \omega_\theta)$ are velocity and vorticity in axial and azimuthal directions (x, θ). In this criterion, as will be seen, the instability waves and the mean vortex lines wind in the same direction, as observed. An alternative description proposed by Ludwieg (1961, 1964) gives the oposite result as well as predicting stability for the present experimental profiles. C_x, C_θ, the minimum of K_{HG}, the angle the most unstable wave $tg^{-1}(-m/kr) = tg^{-1} - G$ corresponding to $min(K_{HG})$ and the angle of the vortex lines of the mean flow $tg^{-1}\omega_x/\omega_\theta = tg^{-1}[-(1+C_\theta)/C_x]$ were calculated as a function of radius for strongly swirling jets before and after breakdown (figure 13a b). In this representation the flow is centrifugally stable if $1 + C_\theta \geqslant 0$ and centrifugally unstable if $1 + C_\theta < 0$, and the flow is locally temporally stable if $min(K_{HG}) \geqslant 0$.

By definition in this formulation the helical waves and the mean vortex lines are co-winding if their angle of inclination is positive and are counter-winding if negative. The inlet region for flow before breakdown and the wake region around the stagnation point for flow after breakdown are most the likely locations for instability initiation and they were chosen for further study. The results were calculated from the mean axial velocity at $S = 0.78$ and 0.9 and from the mean azimuthal velocity at $S = 0.78$ and 0.98 (figure 10). The data were not taken simutaneously due to technical limitations. Agreement can be

found between the present experiments and Howard and Gupta's theory on instability in the outer shear layer, $r \geqslant 0.97R$ at $x = 0D$ for $S = 0.78$ and $r \geqslant 1.43R$ at $x = 0D$ for $S = 0.9$, within which the flow becomes unstable and the most unstable helical waves are more aligned with the local vortex (figure 13 *b*). The angle of the most unstable wave varies in the range of -25 to -30^o within the region $r \geqslant 1.08R$ at $x = 0D$ for $S = 0.78$ and the angle is around -9 to -15^o for $r \geqslant 1.45R$ at $x = 0D$ for $S = 0.9$. These estimated angles are close to the value measured in instantaneous images of vortex spirals both before and after breakdown, -28 to -37^o at $S = 0.78$ shown in figure 6 (*a*) and -6 to -10^o at $S = 1.03$ in figure 6 (*b*). It should be noted that the absolute angles of the helical waves both estimated on instantaneous images and calculated from mean velocity profiles at $min(K_{HG})$ are obviously smaller than those of the calculated mean vortex lines, which is around -50^o at $S = 0.78$ and -25^o at $S = 0.9$, as shown in figures 13 (*b*) and 6 (*a b*). Centrifugal instability introduced into Howard and Gupta's calculation and in the present observation is most likely responsible for the departure of helical waves from the existing mean vortex lines and towards the co-winding direction. However, K–H instability dominated these two flows and the helical waves maintained their counter-winding direction. These results are close to those given in LM for velocity profiles that are similar, but not identical, to those used here.

Also support for theories by Martin & Meiburg (1994), Lim & Redekopp (1998), Loiseleux, Delbende & Huerre (2000), Gallaire & Chomaz (2003*a*) and the computations by Ruith *et al.* (2003), for the case of centrifugally unstable, swirling jet/wake can be found in the present experiments and those presented in L and LM all of which concentrated on an exploration of an absolute/convective instability and global-mode description of the flow stability. . Co-rotating, counter-winding helical waves, which were aligned with the mean vortex lines in shear layers between the jet and its surroundings were found to be the most unstable for strongly swirling jets before and after breakdown. Similarily the theory of Loiseleux, Delbende & Huerre (2000) agrees with present experimental observations for non-swirling and weakly swirling jets, in which the axial shear-layer instability leads to vortex rings, $m = 0$, dominating the flow.

Co-rotating and co-winding helical waves were found by the LadHyX group, Billant *et al.* (1998) and Loiseleux & Chomaz (2003) based on observations of a swirling free-jet with subtly different inlet velocity profiles from those of the present experiments. The former found $m = -2$ for moderate Reynolds numbers and $m = -3$ for larger Reynolds number before breakdown. In a further investigation of the same jet by the latter authors, the most unstable helical wave number m ranged from -7 to -1 as S increased. Counter-rotating, co-winding helical waves with high phase speed became the most unstable at large swirl rates just before the onset of breakdown. Recently, Gallaire & Chomaz (2003*b*) applied linear stability analysis to inlet velocity profiles that modeled those of Billant *et al.* (1998) almost exactly and found a co-rotating co-winding mode, $m = -2$, becoming absolutely unstable (AU) for centrifugally unstable jets. This mode had a phase speed 1/3.3 times the rotation rate of the inlet vortex core at the critical swirl number where it became AU. At a similar swirl rate, Loiseleux & Chomaz (2003) found the double helix $m = -2$ co-rotating with the jet with a phase speed 1/3 times the measured rotation rate measured at $x = 22\,\mathrm{mm}$.

It seems likely that due to the subtle differences in the location of the maxima of the azimuthal and axial shear layers the LadHyX group generated waves that were driven by centrifugal instability while ours, with both shear layers coincident, were of the K–H type and simply rolled-up the existing mean vortex lines. This hypothesis is supported, but not confirmed, by some preliminary calculations by Prof. L. G. Redekopp (private communication) in which he found that the nature of the instability depends very critically

on the relative thicknesses and radial displacements of the two shear layers. It should be noted that in the temporal stability study by Gallaire & Chomaz (2003*b*), co-rotating counter-winding modes $m = +1$, $+2$ and $+3$ became unstable but with lower growth rate than those of the modes $m \leqslant 0$. For large swirling rates, the phase speed of $m = +1$ or $+2$ at its most unstable axial wave number, was close to the rotation rate of the inlet, agreeing with the observations of the present experiments. Since, in the temporal stability analysis, m positive waves were found to have smaller growth rates, they were excluded from further study of the absolute/convective nature of the instability.

A spatially developing model of swirling jets has been recently studied by Ruith *et al.* (2003), and the spiral type of breakdown was found to have the same spatial and temporal evolution as that observed in present experiments. There are several things to be noted about this computational work. First of all, velocity profiles of the inflow, i.e. at the spatial origin $x = 0$, were unchanged by the presence of breakdown in contradistinction to the present work. Secondly, the shear-layer of their model was centrifugally stable at the spatial origin $x = 0$, and centrifugal instability was only found around the breakdown bubble at large swirl number. Thus the most general cases of centrifugally unstable swirling jets were excluded by their study. At the same time, they confirmed the notion expounded in Escudier *et al.* (1983) that breakdown itself was the result of a super to sub-critical transition that generated a downstream flow susceptive to intense helical instabilities which was shown to be of the AI type.

This work was supported by National Science Foundation under Grant No. CTS-9523291. Discussions with Professors L. G. Redekopp, F. K. Browand, P. Huerre and J.-M. Chomaz and Dr. F. Gallaire, as well as the technical help of Professors G. R. Spedding and A. M. Fincham are gratefully acknowledged. More detailed experimental results are given in L and a discussion of the instability modes in LM.

REFERENCES

Althaus, W. & Weimer, M. 1998 Review of the Aachen work on vortex breakdown. *IUTAM Symposium on Dynamics of Slender Vortices* 331

Benjamin, T. B. 1962 Theory of the vortex breakdown phenomenon. *J. Fluid Mech.* **14**, 593

Billant, P., Chomaz, J. M. & Huerre P. 1998 Experimental study of vortex breakdwon in swirling jet. *J. Fluid Mech.* **376**, 183

Browand, F. K. & Laufer, J. 1975 The role of large scale structures in the initial development of circular jets. *Turbulence in Liquids, Science* 333

Brown, G. & Lopez, J. 1990 Axisymmetric vortex breakdown Part 2: physical mechanisms. *J. Fluid Mech.* **221**, 553

Chigier, N. A. & Chervinsky, M. R. 1967 Experimental investigation of swirling vortex motion in jets. *Trans. ASME, J. Appl. Mech.* **34**, 443

Chomaz, J.-M., Huerre, P. & Redekopp, L. 1988 Bifurcations to local and global modes in spatially developing flows. *Physical Review Letters* **60**, 25

Delbende, I., Chomaz, J.-M. & Huerre, P. 1998 Absolute/convective instability of the Bachelor vortex. *J. Fluid Mech.* **355**, 229

Escudier, M., Bornstein, J. & Maxworthy, T. 1982 The dynamics of confined vortices. *Proc. R. Soc.* **A335 19**,27

Escudier, M. 1987 Confined vortices in flow machinery. *Ann. Rev. Fl. Mech.* **19**, 27

Farokhi, S., Taghavi, R. & Rice, E. J. 1989 Effect of initial swirl distribution on the evolution of a turbulent jet. *AIAA J.* **27**, 700

Fuchs, V., Ko, K. & Bers, A. 1981 Theory of mode-conversion in weakly inhomogeneous plasma. *Phys. Fluids* **24**, 1251

Fincham, A. M. & Spedding, G. R. 1997 Low cost, high resolution DPIV for measurement of turbulent fluid flow. *Experiments in Fluids* **23**, 449

Grabowski, W. J. & Berger, S. A. 1976 Solutions of the Navier-Stokes equations for vortex breakdown. *J. Fluid Mech.* **75**, 525

Gupta, A. K., Lilley, D. G. & Syred, N. 1984 Swirl flows. *Kent Engl: Abacus* 475

Gallaire, F. & Chomaz, J.-M. 2003*a* Instability mechanisms in swirling flows. *Phys. Fluids* **15**, 2622

Gallaire, F. & Chomaz, J.-M. 2003*b* Mode selection in swirling jet experiments: a linear stability analysis. *J. Fluid Mech.* **494**, 223

Gallaire, F. & Chomaz, J.-M. 2003*c* Experimental study of a free and forced swirling jet. Submitted.

Hall, M. G. 1972 Vortex breakdown. *Annual Review of Fluid Mechanics* **4**, 195

Harvey, J. K. 1962 Some observations of the vortex breakdown phenomenon. *J. Fluid Mech.* **14**, 585

Howard, L. N. & Gupta, A. S. 1962 On the hydrodynamic and hydromagnatic stability of swirling flows. *J. Fluid Mech.* **14**, 463

Huerre, P. & Monkewitz, P. 1990 Local and global instabilities in spatially developing flows. *Ann. Rev. Fl. Mech.* **22**, 473

Huerre, P. 2001 Open shear flow instabilities. *In Perspectives in Fluid Dynamics, a collective introduction to current research. Cambridge University Press*

Kopecky, R. M. & Torrance, K. E. 1973 Initiation and structure of axisymmetric eddies in a rotating stream. *Computational Fluids* **1**, 289

Koch, W. 1985 Local instability characteristics and frequency determination of self-excited wake flows. *J. Sound and Vibration* **99**(1), 53

Kribus, A. & Leibovich, S. 1994 Instability of strong nonlinear waves in vortex flows. *J. Fluid Mech.* **269**, 247

Kurosaka, M., Kikuchi, M., Hirao, K., Yuge, T. & Inoue, H. 2003 Interchangeability of vortex breakdown types. *Experiments in Fluids* **34**, 77.

Lambourne, N. C. & Bryer, D. W. 1961 The bursting of leading-edge vortices: some observation and discussion of the phenomenon. *Aeronautical Res. Council R&M* **36**, 3282

Leibovich, S. 1970 Weakly nonlinear waves in rotating fluids. *J. Fluid Mech.* **42**, 803

Leibovich, S. & Randall, J. D. 1973 Amplification and decay of long nonlinear waves. *J. Fluid Mech.* **53**, 481

Leibovich, S. 1978 The structure of vortex breakdown. *Ann. Rev. Fluid Mech.* **10**,221

Leibovich, S. & Ma, H. Y. 1983 Soliton propagation on vortex cores and the Hasimoto soliton. *Phys. Fluids* **26**, 3173

Leibovich, S. 1983 Vortex stability and breakdown: survey and extension. *AIAA J.* **22**, 1192

Liang, H. 2003 Experimental investigations of swirling jets. *PhD thesis, Univ. Southern California*

Liang, H. & Maxworthy, T. 2004 An experimental investigation of swirling jets. *submitted to JFM* (http://www-rcf.usc.edu/~ hanzhuan/publications/jfm1.pdf)

Lim, D. & Redekopp, L. 1998 Absolute instability conditions for variable density, swirling jet flows. *Eur. J. Mech., B/Fluids* **17**, 165

Loiseleux, Chomaz, J.-M. & Huerre, P. 1998 The effect of swirl on jets and wakes: linear instability of the Rankine vortex with axial flow. *Phys. Fluids* **10**, 1120

Loiseleux, T., Delbende, I. & Huerre, P. 2000 Absolute and convective instabilities of a swirling jet/wake shear layer. *Phys. Fluids* **12**, 375

Loiseleux, T. & Chomaz, J.-M. 2000 Breaking of rotational symmetry in a swirling jet experiment. Submitted to *Experiments of Fluid*

Loiseleux, T. & Chomaz, J.-M. 2003 Breaking of rotational symmetry in a swirling jet experiment. *Phys. Fluids* **15**, 511

Lucas, K. 1997 Numerical investigation of three-dimensional vortex breakdown. *PhD thesis, Stanford Univ.*

Ludweig, H. Z. 1961 *Flugwiss.* **9**, 359

Mahesh, K. 1996 A model for the onset of breakdown in an axisymmetric compressible vortex. *Phys. Fluids* **8**, 3338

Mankbadi, R. R. 1985 On the interaction between fundamental and subharmonic instability waves in a turbulent round jet. *J. Fluid Mech.* **160**, 385

Martin, J. & Meiburg, E. 1994 On the stability of the swirling jet shear layer. *Phys. Fluids* **6**, 424

Maxworthy, T., Hopfinger, E. J. & Redekopp, L. G. 1985 Wave motions on vortex cores. *J. Fluid Mech.* **151**, 141

Monkewitz, P. A. 1988 The absolute and convective nature of instability in two-dimensional wakes at low Reynolds numbers. *Phys. Fluids* **31**, 999

Panda, J & McLaughlin, D. K. 1994 Experiments on the instabilities of a swirling jet. *Phys. Fluid* **6**, 263

Pier, B., Huerre, P. & Chomaz, J.-M 2001 Bifurcation to fully nonlinear synchronized structure in slowly varying media. *Physica D* **148**, 49

Pier, B. & Huerre, P. 2001 Nonlinear self-sustained structures and fronts in spatially developing flows. *J. Fluid Mech.* **435**, 145

Randall, J. D. & Leibovich, S. 1973 The critical state: a trapped wave model of vortex breakdown. *J. Fluid Mech.* **53**, 495

Ruith, M. R., Chen, P., Meiburg, E. & Maxworthy, T. 2003 Three-dimemtional vortex breakdown in swirling jets and wakes: direct numerical simulation. Submitted to *J. Fluid Mech.*

Sarpkaya, T. 1971 On stationary and travelling vortex breakdown. *J. Fluid Mech.* **45**, 545

Spall, R. E., Gatski, T. B. & Grosch, C. E. 1987 A criterion for vortex breakdown. *Phys. Fluids* **30**(11), 3434

Squire, H. B. 1962 Analysis of the vortex breakdown phenomenon. *Miszellaneen der Angewandten Mechanik, Akademie-Verlag, Berlin* 306